BIOELECTRICITY
Volume 2, Number 4, 2020

DOI: 10.1089/bioe.2020.0019

# Optimization of Electrical Stimulation for Safe and Effective Guidance of Human Cells

Zhiqiang Zhao, PhD,[1,*] Kan Zhu, PhD,[1,2,*] Yan Li, MD,[1] Zijie Zhu, PhD,[3] Linjie Pan, PhD,[4] Tingrui Pan, PhD,[2] Richard B. Borgens, PhD,[4,5] and Min Zhao, MD, PhD[1,2]

**Abstract**

Direct current (DC) electrical stimulation has been shown to have remarkable effects on regulating cell behaviors. Translation of this technology to clinical uses, however, has to overcome several obstacles, including Joule heat production, changes in pH and ion concentration, and electrode products that are detrimental to cells. Application of DC voltages in thick tissues where their thickness is >0.8 mm caused significant changes in temperature, pH, and ion concentrations. In this study, we developed a multifield and -chamber electrotaxis chip, and various stimulation schemes to determine effective and safe stimulation strategies to guide the migration of human vascular endothelial cells. The electrotaxis chip with a chamber thickness of 1 mm allows 10 voltages applied in one experiment. DC electric fields caused detrimental effects on cells in a 1 mm chamber that mimicking 3D tissue with a decrease in cell migration speed and an increase in necrosis and apoptosis. Using the chip, we were able to select optimal stimulation schemes that were effective in guiding cells with minimal detrimental effects. This experimental system can be used to determine optimal electrical stimulation schemes for cell migration, survival with minimal detrimental effects on cells, which will facilitate to bring electrical stimulation for *in vivo* use.

**Keywords:** electrical stimulation, pulsed electric fields, cell migration, multifield electrotaxis chips, endothelial cells, cell damage

## Introduction

Applied direct current (DC) electric fields (EFs) may regulate the direction of cell migration, the orientation of long axis of cells, and the axis of cell division.[1–8] These cellular behaviors are critical for wound healing and tissue regeneration.[9–12] Electric stimulation has many inherent benefits, for example, the stimulation can be switched on and off at desired intervals, with precisely controlled amplitude and direction.[6,13,14] Those benefits will complement chemical treatment, which may be difficult to establish stable and directional gradients *in vivo*. If the DC electrical stimulation can be successfully used *in vivo*, it would offer a powerful modality to facilitate treatment of many important diseases, to repair, and to regenerate damaged tissues.

However, application of DC EFs to live tissue inevitably causes significant changes in local environments that are detrimental to cells.[15,16] Maintaining DC voltages similar to that we normally apply to cells in dish induces significantly larger currents in live tissues, because of the 3D bulk tissues provide much lower resistance compared with the electrotaxis chamber we normally use.[17] Larger currents generate significantly more heat—Joule's effect, which cannot dissipate effectively. Larger currents also generate significantly more electrode products that are toxic to tissues—for example, changes in pH, and concentrations of $Ca^{2+}$, $Na^{+}$, $K^{+}$, and others ions.[6,11] Previous studies have shown when DC voltages are applied to electrotaxis chambers thicker than 0.8 mm, or specimens thicker than 0.4 mm, changes in pH, [$Ca^{2+}$], and temperature are inevitable.[15]

[1]Department of Ophthalmology & Vision Science, Department of Dermatology, Institute for Regenerative Cures, University of California Davis, Sacramento, California, USA.
[2]Department of Ophthalmology, University of California Davis, School of Medicine, Sacramento, California, USA.
[3]Department of Biomedical Engineering, University of California Davis, Davis, California, USA.
[4]Center for Paralysis Research, Department of Basic Medical Sciences, College of Veterinary Medicine, Purdue University, West Lafayette, Indiana, USA.
[5]Weldon School of Biomedical Engineering, Purdue University, West Lafayette, Indiana, USA.
*These authors contributed equally to this article.

Developing methodology to determine safe and effective electrical stimulation schemes for *in vivo* use will, therefore, facilitate translation of electrical stimulation to clinical use. In this study, we developed a multifield and -chamber electrotaxis chip, and optimized stimulation schemes for effective and safe electrical guidance of cells. We chose vascular endothelial cells for our experiments, because endothelial cells, similar to many types of cells, respond to physiological EFs with a directed migration (electrotaxis/galvanotaxis).[6,11,18–20] Directional migration of endothelial cells and new blood vessel formation are critical in wound healing and tissue regeneration.[21–23] DC EFs also guide migration of endothelial cells.[24,25] The use of electric stimulation for directed endothelial cell migration during angiogenesis may have profound implications for manipulation of many important diseases.

Herein, we determined optimal stimulation scheme for guidance of human endothelial cells (HUVEC), while minimizing cell apoptosis and necrosis. The effectiveness of selected pulsed fields was compared with that of DC voltages in the same culture system. These results provide a basis for future development of stimulation schemes to guide cell migration in thick tissues and *in vivo*.

## Materials and Methods

### *Materials*

Sylgard 184 silicone elastomer (polydimethylsiloxane/PDMS) was purchased from Dow Corning (USA). Dulbecco's modified Eagle's medium (DMEM), $CO_2$ independent medium, fetal bovine serum (FBS), D-PBS, trypan blue solution, and Hoechst 33342 nucleic acid stain were from Life Technologies (USA). Annexin-V apoptosis kit was from Roche (USA). FNC coating mix was from AthenaES (USA). Agar was purchased from Sigma-Aldrich (USA). Silver wires with 99.999% purity were purchased from Advent Research Materials Ltd. (UK).

### *Cell culture*

HUVEC were from American type culture collection (ATCC, USA). Cells were cultured in DMEM supplemented with 10% (v/v) FBS, 1% (v/v) penicillin and streptomycin at 37°C in 5% $CO_2$ incubator. All experiments were performed within passage 10.

### *Design and fabrication of multifield and -chamber electrotaxis chip*

Our multifield electrotaxis chip is designed based on the R–2R resistor ladder structure as described previously.[26] In brief, the resistor ladder structure consists of repeating identical units of current dividers, each of which uses one series resistor of R and one shunt resistor of 2R, as shown in Supplementary Figure S1. As the input current reaches the first unit, it experiences an equal split (in the dotted box of Supplementary Fig. S1) between the series ($I_S$) and the shunting ($I_T$) paths due to the impedance matching between these two paths, and thus only half of the input current flows down to the next stage. The repeated R–2R resistor unit establish logarithmic series of voltage gradients with a common ratio of 2 (Supplementary Fig. S1). And that made it an infinitely expandable voltage builder that depends on the requirement of experiment. In the reported chips, the voltage gradient ratio was $2^9{:}2^8{:}\cdots{:}2^1{:}2^0$. The shunt resistor at the last unit is set to be R to terminate the sequence.

Moreover, the voltage gradient is solely dependent on the ratio of the two resistors rather than their actual values. The microfluidic resistors are constituted by microchannels filled with conductive electrolyte solutions (e.g., cell culture medium). The electrical resistance can be easily adjusted by changing the microchannel dimensions, following Ohm's law. In this study, two types of chips were designed and fabricated, where their chamber height was different, thick chamber with height of 1 mm, and thin one with height of 0.4 mm. The 1 mm chamber would mimic live tissue; the 0.4 mm one was the regular electrotaxis chamber most laboratories routinely use for electrotaxis experiments.

The reported multifield chip comprised two PDMS layers and plastic culture dish. The top layer formed the ''roof'' of electrotaxis chambers (Fig. 1B–D and Supplementary Fig. S2A). The middle layer formed the ''wall'' of electrotaxis chambers. The bottom was plastic cell culture dish, on which cells were seeded. Once assembled, the chips had multiple chambers, and also had two connecting pools for the medium and the agar bridges. The dimension of each chamber in thick chips was 1 mm (width) × 1 mm (height) × 5 mm (length); the thin one was 1 mm (width) × 0.4 mm (height) × 5 mm (length) (Fig. 1E).

The two-layer PDMS structure was fabricated and assembled by employing standard laser micromachining and oxygen plasma-assisted bonding.[26] Immediately before cell seeding, FNC coating mix was coated on the surface of culture dish. Then the sterile two-layer structure was assembled into culture dish to form a finished chip (Fig. 1C).

### *Simulation and measurement of EF distribution in the multichamber chip*

The simulation of voltage distribution was performed in a stationary condition with a conductivity of the NaCl solution of 1.408 S/m (25°C). It was focused on the EF distribution inside the multichamber electrotaxis chips. Both 1 and 0.4 mm chips were modeled for the simulation. COMSOL Multiphysics 4.3 was used for modeling and simulation.

To confirm the simulation, we embedded Ag/AgCl electrodes through the upper PDMS layer and connected with a digital multimeter. Based on the design and simulation, a DC voltage of 6 V in total were applied between the two ends of the left channel in Figure 1C. Actual DC voltages across each chamber were measured.

### *System for electrotaxis study*

Supplementary Figure S2B shows the configuration of the entire system.[15] The system consisted of a multifield and -chamber chip, two agar salt bridges, a power supply, an X–Y motor stage, and an inverted microscope (Zeiss) equipped with digital camera (not shown in Supplementary Fig. S2B). The X–Y stage was controlled by a MetaMorph imaging software (Molecular Devices, USA).

### *Selected pulsed EF stimulation scheme*

The selected pulsed EF stimulation scheme 1 (PEF s1) was a bipolar pulsed EF scheme, which included (i) positive on time 200 ms, (ii) positive off time 20 ms, (iii) negative on time 20 ms,

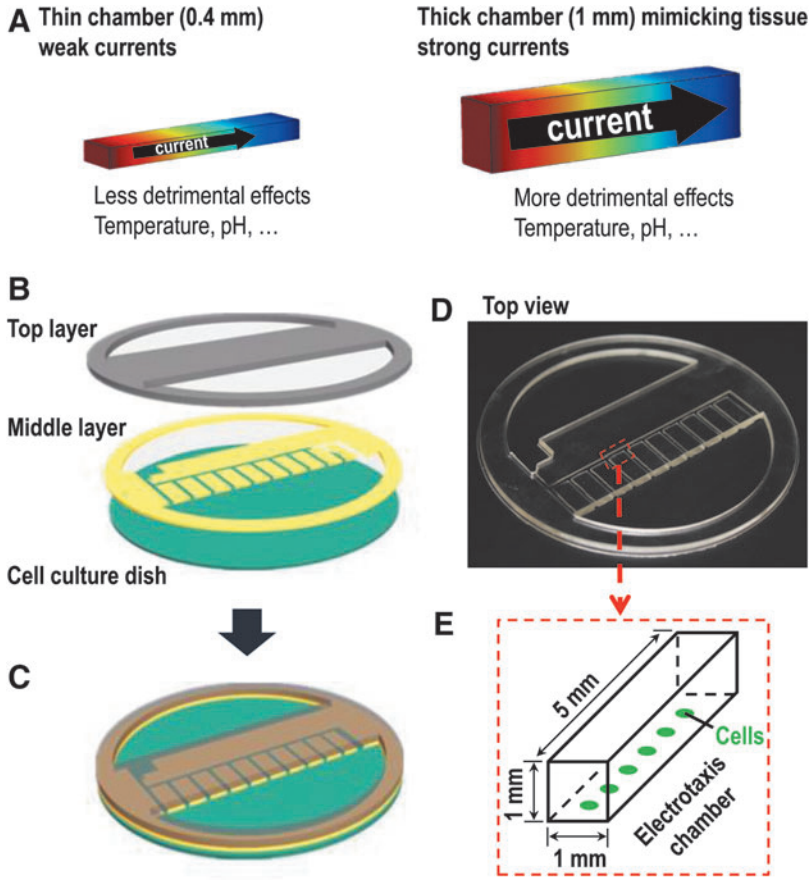


**FIG. 1.** Design of a multifield and -chamber chip. **(A)** Schematic diagraphs showing effects of the thickness of electrotaxis chamber on electric currents, Joule heating, and changes in pH and concentration of ions. Currents and Joule heating effect increase proportionally with the tissue thickness, thus the detrimental effects caused. **(B)** A 3D illustration showing the three-layer structure of the chip. **(C)** A schematic diagraph showing the assembled chip in working condition. **(D)** Top view of the assembled chip includes top layer and middle layer. **(E)** The dimension of each electrotaxis chamber in the chip. Cells were seeded on the culture dishes.

and (iv) negative off time 20 ms (Fig. 2A). The positive stand for anode, and current flowed from anode to cathode in the electrotaxis chambers. The negative stand for reversed polarity of EF, and current flowed from new anode to new cathode in the chamber. The duty cycle of PEF s1 was 85%, and the frequency was 3.8 Hz. It was generated by a custom-designed programmable bipolar current generator as described previously.[14]

The pulsed EF stimulation scheme 2 (PEF s2) was modified from PEF s1. It had same positive on time with PEF s1, but without negative current. The frequency was 3.8 Hz, same with PEF s1. It included (i) positive on time 200 ms and (ii) positive off time 60 ms. Therefore, it was a single polar pulsed EF (Fig. 2B). It was generated by the bipolar current generator too.[14] The duty cycle was 77%.

The selected pulsed EF stimulation scheme 3 (PEF s3) was also a single polar pulsed EF, which included positive on time 15 min and positive off time 8 min (Fig. 2C). Within a 4 h of experimental running time, the duty cycle of PEF s3 was 67%, and the frequency was 0.0007 Hz. It was generated by a programmable DC power supply (Chroma System Solutions, USA).

### *Cell migration and electrotaxis assay*

Cell migration assay was performed using the multifield electrotaxis chips (Fig. 1 and Supplementary Fig. S2).[27] The chip automatically generates multifield gradients when a voltage is applied (Fig. 3A; see also in Results).

Cells with a density of $1 \times 10^4$ cells/mL were seeded and allowed to grow for at least 12 h in the multifield chips in growth medium at 37°C in a 5% $CO_2$ incubator. Immediately before a test, growth medium was replaced with $CO_2$-independent medium [supplemented with 10% (v/v) FBS, 1% (v/v) penicillin and streptomycin]. For EF application, a voltage was applied through agar-salt bridges connecting silver/silver chloride electrodes in beakers of Steinberg's solution as previously described[15] to pools of medium on either side of the chip (Supplementary Fig. S2). Agar gel was preprepared in a sterilized condition by dissolving 5% (wt/vol) agar powder (Sigma, catalog no. A1296) into Steinberg's solution. Cells were exposed to a DC EF or a pulsed EF for 4 h as indicated at 37°C in a temperature-controlled hood on an inverted microscope stage. Serial time-lapse images were recorded using a Zeiss Observer Z1 inverted microscope and MetaMorph imaging system.

### *Quantification of cell migration*

Directional cell migration was quantified as directedness and migration speed by tracing the position of cell nuclei relative to their original position at $T=0$, at a frame interval of 5 min using the Image J software (NIH). The directedness of migration was defined as cosine $\theta$, where $\theta$ is the angle between the EF vector and a straight line connecting the start and end position of a cell.[11] A cell moving directly toward the anode would have a directedness of 1; a cell moving directly along the field lines toward the cathode would have a directedness of −1; a mean value close to 0 represents random cell movement. The cosine $\theta$ will provide a number between −1 and +1 and the average of all the separate cell events

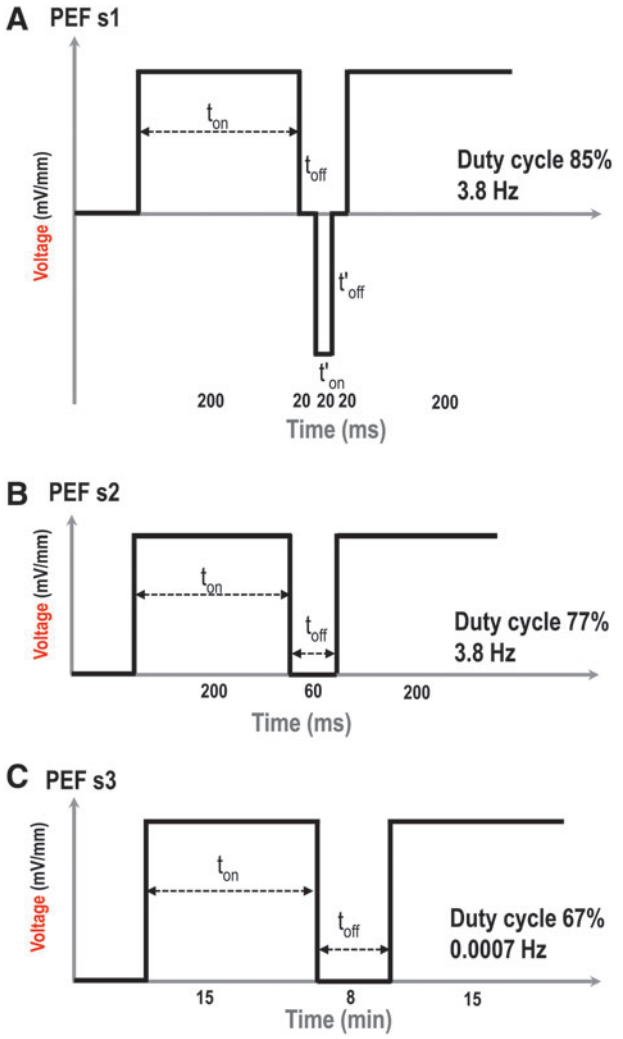


**FIG. 2.** Schematic diagrams of three selected pulsed EF stimulation schemes. **(A)** Pulsed EF scheme 1 (PEF s1). **(B)** Pulsed EF scheme 2 (PEF s2). **(C)** Pulsed EF scheme 3 (PEF s3). $t_{on}$: duration of time when stimulation was switched on; $t_{off}$: duration of time when stimulation was switched off. The duty cycle and frequency of the selected stimulation schemes were as shown.

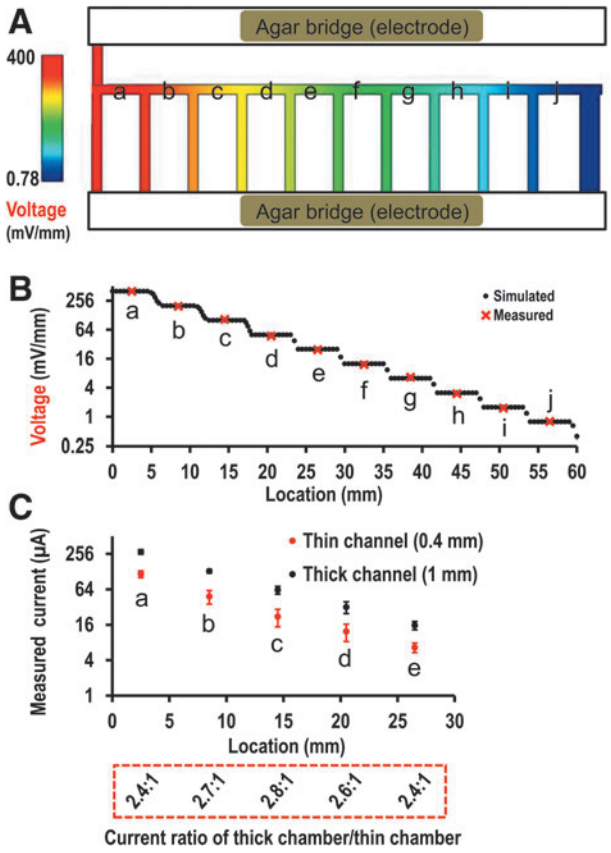


**FIG. 3.** Multiple fields generated in the chip. **(A)** Simulated voltage gradient in the multifield chip. The maximum field was in chamber (a) on the left, in red; the minimum field was in chamber (j) on the right, in dark blue. **(B)** Simulated and measured field strength from chamber (a) to chamber (j). The field dropped down 50% chamber by chamber from (a) to (j). **(C)** Electrical currents experimentally measured in the chambers (a) to (e) either with 1 mm or 0.4 mm chamber. A larger current was on the 1 mm chamber, and a smaller current was on the 0.4 mm chamber. Value in red box was the ratio of current (1:0.4 mm), which was close to 2.5:1. The current from either 1 mm chamber or 0.4 mm chamber dropped down 50% chamber by chamber from (a) to (e). The measurement in chamber (g) to (j) was not shown because they were very small and quite close to *X* axis in the plot.

yields an average directedness index. The average directedness of a population of cells gives an objective quantification of how cells have moved in relation to the EF vector.

The migration speed is the total length of the trajectory that a cell has migrated divided by the time. Migration distance over X axis is the projection of the cell trajectory on the *X* axis, which represents the migration of cells along the EF vector.

### *Measurement of pH and temperature*

In the chips either with thin channels or thick channels, a small window with a radius of 0.5 mm was opened in the ''roof'' of electrotaxis channel. Either before or after EF application, pH was measured through the window by pH indicator papers (Sigma, USA). The temperature of culture medium was measured by an Infrared Thermometer (Prizm Medical, USA).

### *Apoptosis and necrosis assay*

We used the Annexin-V-FLUOS staining kit (Roche) to determine cell apoptosis and necrosis rate. Annexin-V could preferentially bind to phosphatidylserine, a marker of apoptosis when it is on the outer leaflet of the plasma membrane.[28] Propidium iodide (PI) is a red-fluorescence dye that only permeant to dead cells. Cells were rinsed with cold PBS and fixed in 4% paraformaldehyde at 4°C for 30 min immediately after electrical stimulation. Normal, apoptotic, and dead cells were distinguished by fluorescence microscopy.

### *Statistical analysis*

Data are reported as mean ± standard error of the mean, with *n* denoting the number of tests except in the migration assay where *n* denotes the number of cells. Means were compared using one-way analysis of variance in group comparison. Two-tailed Student's *t*-test for unpaired data

was applied as appropriate. A value of $p < 0.05$ was considered statistically significant.

## Results and Discussion

### *Stable multifields in the chip with increased chamber height and currents*

A numerical simulation of the EF distribution in the multifield and -chamber chips is shown in Figure 3. A DC voltage gradient where their strength dropping down 50% one chamber by one chamber from chamber (a) down to chamber (j) is expected theoretically (Fig. 3A, B and Supplementary Fig. S3). Homogeneous EFs were observed by simulation in each chamber of the chip. In this study, a voltage of 400 mV/mm was applied in the chamber (a). Theoretically, the voltage gradient obtained by simulation would be 400, 200, 100, 50, 25, 12.5, 6.25, 3.125, 1.5625, 0.78125 mV/mm (Fig. 3B). The actual EF strength was measured as shown in Figure 3B. The result shows that the measured voltage corresponds well to the simulated value.

We previously reported that this multifield device is capable of screening cell migration under the stimulation of a voltage gradient spanning over three orders of magnitude; however, the directional responses of human corneal cells rapidly decreased in higher voltages >400 mV/mm.[26] We hypothesize that high voltages may induce some side effects due to the changes in pH, [Ca2+], and temperature, and reducing the chamber thickness may improve the directional responses. Thus, chips with two kinds of thickness, 1 and 0.4 mm were fabricated for the study (Fig. 1D, E). The 1 mm chambers filled with culture medium will have electric currents flowing through significantly larger than that through the 0.4 mm chambers. At the same voltage, the 1 mm chamber, therefore, produces more Joule heat, more changes of pH, temperature, and ion concentration in the culture medium than that of 0.4 mm one (Fig. 1A).[15] Based on the Pouillet's law, the electrical resistance ($R$) of culture medium decreases with the increase of the thickness/height of the chamber (Supplementary Fig. S3A). Based on the Ohm's law, the electrical current through a bulk material in the electrotaxis chamber is $I = V/R$, where $V$ is the potential difference measured across culture medium. The electrical current increases with increasing the thickness/height of the chamber (Supplementary Fig. S3B). Joule's first law states that the amount of heat (Joule heating) generated by an electric current through a bulk material $Q = I^2 \cdot R$. The heat generated thus increases with increasing the thickness/height of the chamber (Supplementary Fig. S3C). In our study, the electrical currents in both chips were experimentally confirmed with measurements when same EFs were applied (Fig. 3C). The height ratio of two chips was 2.5:1 (1 mm/0.4 mm). The ratio of measured electrical currents was close to 2.5:1. Therefore, the currents increased with the height of chamber as we designed for and expected.

The multifield and -chamber electrotaxis chips offer an effective tool to perform cell migration assay. Comparing the electrotaxis chambers reported before, the reported chips in this study have some advantages. Compared with previously reported multifield chip,[2] our setup of multifield is infinitely expandable without increasing total power consumption. Cell responses to voltage gradients ranging over three orders of magnitude can be tested in a single experiment. Besides, the thickness of the chip is precisely controlled and adjustable to mimic any *in vivo* live tissue microenvironment.

### *Increasing chamber thickness resulted in apoptosis and necrosis in DC EFs*

Cell migration response to DC EFs was determined with either 1 mm chips or 0.4 mm chips (Fig. 4 and Supplementary Fig. S4). In the control (0 mV/mm), endothelial cells (HUVEC) migrated randomly. In the presence of DC EFs, cathodal directed cell migration was evident at a voltage of 100 mV/mm (Fig. 4A, B and Supplementary Fig. S4; $p < 0.05$, compared with 0 mV/mm). Increasing voltage increased cathodal cell migration directedness (Fig. 4B). The migration speed was also increased by DC EFs and peaked at a voltage of 400 mV/mm in 0.4 mm chamber chips (Fig. 4A; $p < 0.001$, compared with 0 mV/mm). However, in a voltage of 200 mV/mm in the 1 mm chamber, cell migration speed dropped down significantly. In the 0.4 mm chamber chips, cell response to DC EFs was consistent and stable. In the presence of a voltage of either 200 or 400 mV/mm, cell migration speed was increased comparing with either no field-treated (0 mV/mm) control cells or that of same field on 1 mm chips (Fig. 4A; $p < 0.001$).

Cell damage was assessed by the percentage of cell apoptosis and cell necrosis. We referred to conditions as ''safe'' if cell apoptosis and cell necrosis were <10%. In the 1 mm chips, in the presence of DC voltages up to 100 mV/mm, <10% of total cells were either apoptotic cells or necrotic cells (Fig. 4C, D). In the presence of DC voltage either 200 or 400 mV/mm, however, >70% cells were either apoptotic or necrotic (Figs. 4C, D and 6A; $p < 0.05$, compare with 0 mV/mm). In the 0.4 mm chips, up to 400 mV/mm, no significant numbers of apoptotic or necrotic cells were found (Fig. 4C, D).

In 1 mm chips (chamber height 1 mm), a DC voltage of 200 or 400 mV/mm induced cell damaged in $\sim$70% of total visualized cells. Contrastingly, cells in the 0.4 mm chamber chips (chamber height 0.4 mm) maintained robust response to DC voltages and showed no sign of damage at same voltages. The 1 mm chamber indeed had increased current and Joule heating and other effects that resulted in cell damage. One solution was to reduce the exposure time of EFs.

Electrotaxis responses of different types of cells are varied when exposed to EFs, in which most of the cells migrate directionally to the cathode, whereas some other types move to the anode,[11,29,30–32] and even the same type of cells can switch migration directionality depending on EF strength.[33] The HUVECs migrated to the cathode in this study. Intriguingly, our previous study showed that a different line of human ECs migrated to the anode.[34] The varied cell electrotaxis responses may be due to different lines and/or other conditions. We previously reported a compass model of electrotaxis that governed by two competing pathways, PI3K and myosin, to control cell migration directions.[35] Second messengers,[36,37] for example, cyclic guanosine monophosphate and its phosphatidylinositol signaling, integrins,[38] and surface electrical properties[39] have also been proposed in different cell models as the directional determinants during electrotaxis. However, the key mechanism controlling cell migration directions in EFs still remains uncertain and further studies are needed.

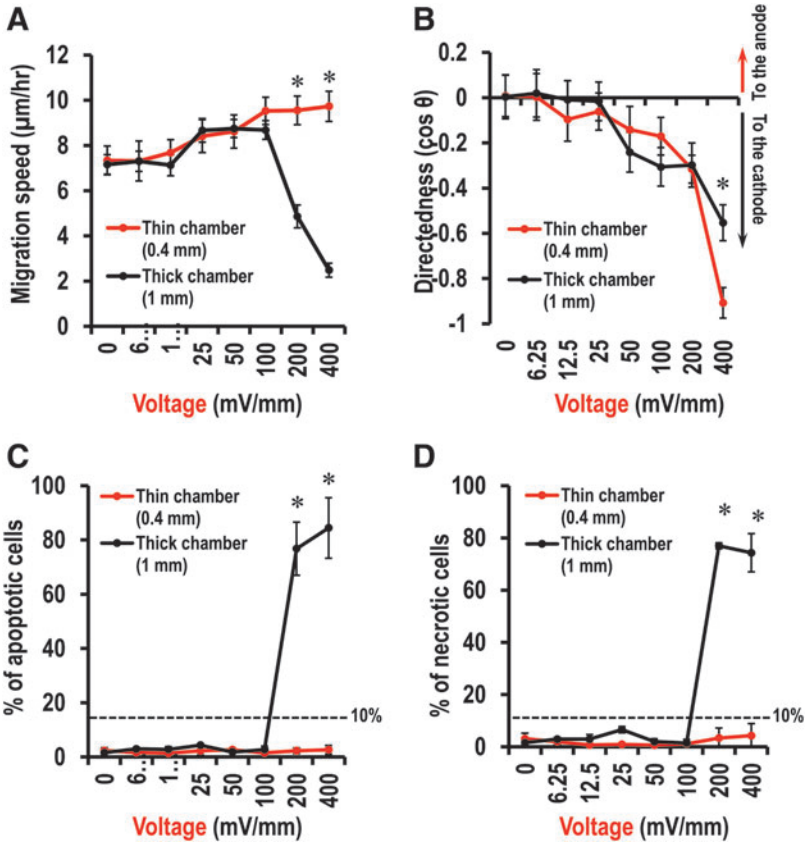


**FIG. 4.** Endothelial cells response to EFs in thin and thick chambers. **(A)** Cell migration speed. **(B)** Cell migration directedness. **(C)** Percentage of apoptotic cells. **(D)** Percentage of necrotic cells. Data are shown as mean ± SEM of three independent experiments. Numbers of cells analyzed have been shown in Supplementary Tables S1 and S2. *$p < 0.05$, when compared with the thick chambers (1 mm) using Student's *t*-test. EFs, electric fields; SEM, standard error of the mean.

### *Pulsed EFs-guided cell migration*

Three pulsed EF schemes were applied, respectively, with 1 mm chamber chips. Cell response to DC EFs acted as a control group (Fig. 5 and Supplementary Figs. S5, S6). In the presence of PEF s1, in a voltage of 400 mV/mm, either cell migration distance over the *X* axis toward cathode or cell directedness index was significantly increased comparing with the DC EF-treated group ($p < 0.05$; Fig. 5B, C and Supplementary Figs. S5, S6B). In the three pulsed EF-treated group, in a voltage of 200 or 400 mV/mm, cell migration speed was significantly increased comparing with the DC EF-treated group ($p < 0.05$; Fig. 5F). Moreover, in presence of PEF s1 and PEF s2, in a voltage of either 200 or 400 mV/mm, cell migration speed was significantly increased comparing with no field-treated group ($p < 0.05$; Fig. 5F). However, in the presence of PEF s3, in a voltage of either 200 or 400 mV/mm, cell migration speed was not increased comparing with no field-treated group (Fig. 5F). This suggested that, as expected, pulsed EF schemes maintained a guided cell migration up to a voltage of 400 mV/mm.

Next, both cell migration speed and cell migration distance over the *X* axis in a voltage of 400 mV/mm were broken down to further compare guiding cell migration effect of three pulsed EF scheme (Supplementary Fig. S6). Within 240 min (4 h), in the presence of three pulsed EF schemes, cells maintained a faster migration speed comparing with the DC EF-treated group ($p < 0.05$; Supplementary Fig. S6A). Especially, during 20–40 min, in the presence of PEF s1, cell showed fastest migration speed (Supplementary Fig. S6A). During 0–40 min, in the presence of PEF s1, cells showed the largest migration distance over the *X* axis toward cathode (Supplementary Fig. S6B). This indicated that pulsed EF schemes maintained a directional cell migration in a range of voltages 100–400 mV/mm within 4 h. The PEF s1 offered the best guiding effect within three selected pulsed EF schemes.

Electrical stimulation with different waveforms, including DC, alternating current, and mono- and biphasic pulsed current, have been studied by others in different models to discuss the physiological bases for using exogenously applied EFs to guide and enhance electrotaxis. Li et al. demonstrated that *Dictyostelium* cells had better directional performance under 90% duty cycle pulsed DC EFs and 80% duty cycle bipolar pulse EFs compared with DC EFs.[40] Ren et al. also reported that pulsed EFs could induce robust electrotaxis comparable with or better than that induced by constant DC EFs, which depends on voltage and duty cycle.[41] Pulsed EFs have also been shown induce more effective electrotactic movement of *Caenorhabditis elegans* and *Caenorhabditis briggsae*.[42,43] Moreover, *in vivo* wound interventions with electrical stimulations of different waveforms have been developed and tested with standard wound care and reported to enhance wound healing.[44,45] These findings support our results and suggest that pulsed EFs are vital to electrotaxis and promising in both basic and clinical researches.

### *Pulsed EFs reduced cell damage*

To further assess the difference between pulsed EFs and DC EFs, we examined cell damage using Annexin-V and PI to stain apoptotic cells and necrotic cells, respectively, in 1 mm chamber chips after electrical stimulation. In the

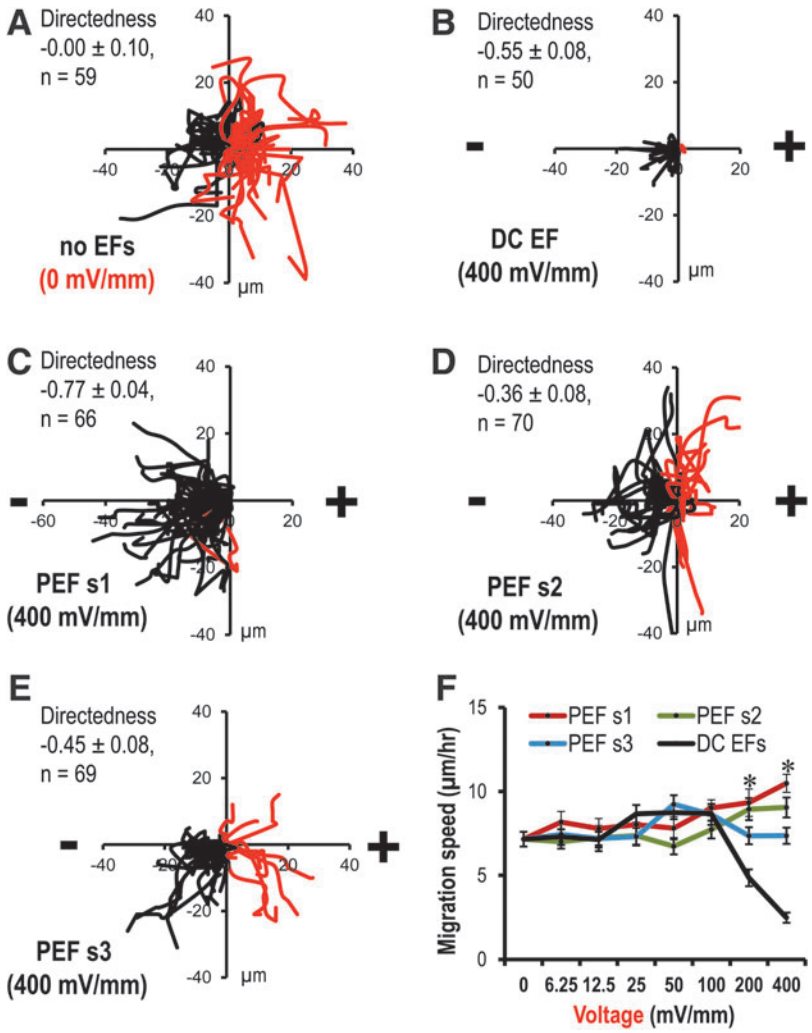


**FIG. 5.** Selected results showing stimulation schemes-guided cell migration with minimal detrimental effects. **(A–E)** Composite graphs of cell trajectories. Black line, cells migrated to the left; red line, to the right. **(A)** In the absence of EFs (0 mV/mm), cells migrated randomly. **(B)** In the presence of a DC EF, cells migrated to the cathode, but due to side effects, cell motility was significantly decreased. **(C)** In the presence of a PEF s1, cells migrated to the cathode. Cell directionality was significantly increased than that in DC EFs. **(D)** In the presence of a PEF s2, cells migrated to the cathode. Cell directionality was smaller than that in DC EFs. **(E)** In the presence of a PEF s3, cells migrated to the cathode. Cell directionality was smaller than that in DC EFs. **(F)** Cell migration speed with either a DC EF or three pulsed EF stimulation schemes. In the presence of a PEF s1, cell migration speed was significantly increased than that of in DC EFs. No EF-treated (0 mV/mm) cells were used as a negative control. Data are shown as mean ± SEM of three independent experiments. Numbers of cells analyzed have been shown in Supplementary Table S3. $*p < 0.05$, when compared with DC EFs using Student's *t*-test. DC, direct current; PEF s1, pulsed EF stimulation scheme 1.

presence of a DC voltage of 400 mV/mm, >70% of cells were either apoptotic or necrotic (Fig. 6; see also in Fig. 4C, D). However, most of the cells were not labeled by Annexin-V or PI (Fig. 6A), and the quantification data showed that >90% of total cells in the visual fields were neither apoptotic cells nor necrotic cells after 4 h of pulsed EF stimulation up to a voltage of 400 mV/mm (Fig. 6C, D and Supplementary Fig. S7). This indicated that pulsed EF schemes of the same voltage could reduce the side effects, which would cause cell damage after a prolonged exposure while maintaining comparable electrotactic responses.

### *Pulsed EFs reduced changes in pH and Temperature*

The pH and temperature were measured and reordered before a voltage of 400 mV/mm application and after that with 1 mm chips. In no field-treated group, the pH and temperature in the center of electrotaxis chamber did not change significantly (Fig. 6D, E).

In the presence of PEF s1, the pH and temperature did not significantly change either (Fig. 6D, E), which confirmed the theoretical idea that negative current could reduce the toxic reactive products generating during the positive current application. By contrast, in the DC EF-treated group, the pH significantly changed, and dropped down to 6.7 ± 0.3 (Fig. 6D; $p < 0.05$, compared with either field-treated before 8.1 ± 0.4 or no field-treated (0 mV/mm) control group 8.0 ± 0.4). In the DC EF-treated group, the temperature was significantly increased to 39.3 ± 0.5°C (Fig. 6E; $p < 0.05$, compared with either field-treated before 36.5 ± 0.5°C or no field-treated (0 mV/mm) control group 36.6 ± 0.5°C). This indicated that pulsed EF scheme 1 could minimize pH change and heat generation in 3D culture.

Three pulsed EF stimulation scheme reduced EF exposure time down to 85% (PEF s1), 77% (PEF s2), and 67% (PEF s3), respectively (Fig. 2), In three pulsed EF stimulation schemes, with 1 mm chips, cells exhibited cathodal migration and their migration speed was increased with voltage, which was similar with that of 0.4 mm chips in DC EFs-treated group (Figs. 4A and 5F). Cell damage was also reduced in three pulsed EF schemes (Fig. 6). The changes of pH and temperature of growth medium was reduced too (Fig. 6). Continuous exposure to DC EFs results in accumulation of toxic reactive oxygen species in growth medium and subsequent cell/tissue damage due to the electrochemical reactions that occur in the channels. The pulsed EF stimulation scheme reduces the total EF exposure time and, therefore, reduces the electrical chemistry changes in the channels and stabilizes the Ph.[46–48] It should be noted that there was a short-term negative voltage applied in each cycle of PEF s1. This may help

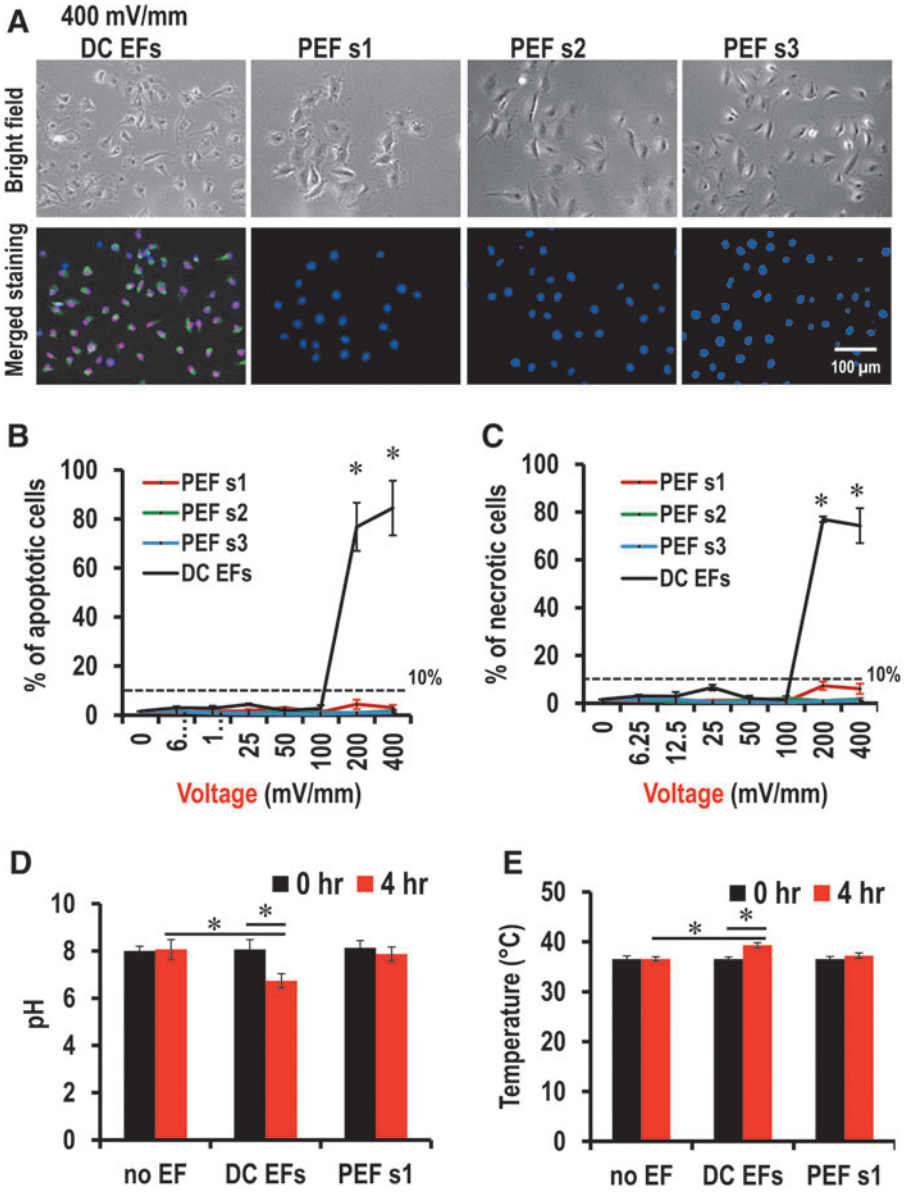


**FIG. 6.** A pulsed EF stimulation scheme has effective guidance with minimized cell damage. **(A)** Assessment of apoptosis and necrosis. Green, apoptotic cells; red, necrotic cells; blue, nucleus. **(B)** Percentage of apoptotic cells. **(C)** Percentage of necrotic cells. **(D)** Measurement of pH before and after EF application. **(E)** Measurement of temperature before and after EF application. No EF-treated (0 mV/mm) cells were used as a negative control. Data are shown as mean ± SEM of three independent experiments. Numbers of cells analyzed have been shown in Supplementary Table S4. $*p < 0.05$, Student's *t*-test.

to eliminate the accumulation of toxic reactive oxygen species and electrical charge during the long-term application of the positive voltage.[14] Therefore, it resulted in a stable pH in the channel (Fig. 5D).

Ren et al. reported that mono pulsed EF with >60% duty cycle induces fewer electrochemical and cytotoxic reactions than a constant DC EF while maintaining robust electrotaxis.[41] Our results confirmed and furthered the finding that pulsed EFs indeed are better stimulation schemes for long-term and effective electrical stimulation, and the biphasic pulsed EF schemes under asymmetric 77% duty cycle would be one of the best options when applying a voltage in thicker chambers for organoids or live tissues. Not only the cell response was maintained, but also the cell damage was reduced. In this study, our results suggested that the safe range of electrical stimulation was extended to 50–400 mV/mm by the pulsed EF scheme. Comparing the three pulsed EF schemes in between, the PEF s1 with a biphasic and asymmetric waveform induced the best directional human cell migration. Using that scheme, Pan et al. has reported that it increased neuron growth rate.[14] In this study, we reported that pulsed EF schemes induced a directed endothelial cell migration and keep cell damage in a safe range.

## Conclusions

We report an experimental method to determine optimal schemes of electrical stimulation that effectively regulate cell migration and other cell behaviors with minimized detrimental effects on cells. The controlled pulse generators produce different wave forms, size of currents, and field strength. The multifield and -chamber electrotaxis chip was designed to mimic passing electric currents through live tissues. Computer simulation and experimental measurements are consistent and can greatly facilitate further design of the system to mimic many other tissue thicknesses. Cell migration, apoptosis, and necrosis staining are sensitive index for detrimental effects on cells.

Our chip design allows significantly increase in the efficiency of determine optimal stimulation schemes in guiding cell migration. Using this method, we demonstrated the detrimental effects systematically of electrical stimulation on cells when the electrical resistance decreases as would be the case when electrical stimulation is applied to tissues *in vivo*. The results showed decreased directional cell responses but increased cell damages in thicker chambers with significantly larger currents, which suggested that decreasing the current while maintaining an optimal voltage would be the key factor for efficient EF stimulation *in vivo*. In addition, we reported the results of four stimulation schemes and determined the optimal stimulation schemes for HUVEC. We demonstrated that the bipolar pulsed EF stimulation schemes with an asymmetric waveform are capable to induce cathodal migration with minimal detrimental effects on apoptosis and necrosis, which would be more suitable for clinical application of electrical stimulation.

### Acknowledgments

We thank Brian Wei (Stanford University) for his valuable technical assistance.

### Author Disclosure Statement

No competing financial interests exist.

### Funding Information

This study was supported by the National Institutes of Health (NIH; 1R01EY019101 and R21EB015737), Air Force Office of Scientific Research (AFOSR; MURI FA9550-16-1-0052), and the Defense Advanced Research Projects Agency (DARPA; HR001119S0027). Work in Zhao Laboratory is also supported by NEI Core Grant (P-30 EY012576, PI. Jack Werner), the Research to Prevent Blindness, Inc.

### Supplementary Material

Supplementary Figure S1
Supplementary Figure S2
Supplementary Figure S3
Supplementary Figure S4
Supplementary Figure S5
Supplementary Figure S6
Supplementary Figure S7
Supplementary Table S1
Supplementary Table S2
Supplementary Table S3
Supplementary Table S4

### References

1. Zhao Z, Watt C, Karystinou A, et al. Directed migration of human bone marrow mesenchymal stem cells in a physiological direct current electric field. Eur Cells Mat 2011;22:344–358.
2. Huang CW, Cheng JY, Yen MH, et al. Electrotaxis of lung cancer cells in a multiple-electric-field chip. Biosen Bioelectron 2009;24:3510–3516.
3. Song S, Han H, Ko UH, et al. Collaborative effects of electric field and fluid shear stress on fibroblast migration. Lab on a Chip 2013;13:1602–1611.
4. Wu D, Ma X, Lin F. DC electric fields direct breast cancer cell migration, induce EGFR polarization, and increase the intracellular level of calcium ions. Cell Biochem Biophy 2013;67:1115–1125.
5. Li Y, Weiss M, Yao L. Directed migration of embryonic stem cell-derived neural cells in an applied electric field. Stem Cell Reviews 2014;10:653–662.
6. McCaig CD, Rajnicek AM, Song B, et al. Controlling cell behavior electrically: Current views and future potential. Physiol Rev 2005;85:943–978.
7. Pullar CE, Baier BS, Kariya Y, et al. Beta4 integrin and epidermal growth factor coordinately regulate electric field-mediated directional migration via Rac1. Mol Biol Cell 2006;17:4925–4935.
8. Mycielska ME, Djamgoz MB. Cellular mechanisms of direct-current electric field effects: Galvanotaxis and metastatic disease. J Cell Sci 2004;117:1631–1639.
9. Martin P. Wound healing—aiming for perfect skin regeneration. Science 1997;276:75–81.
10. Kupperman E, An S, Osborne N, et al. A sphingosine-1-phosphate receptor regulates cell migration during vertebrate heart development. Nature 2000;406:192–195.
11. Zhao M, Song B, Pu J, et al. Electrical signals control wound healing through phosphatidylinositol-3-OH kinase-gamma and PTEN. Nature 2006;442:457–460.
12. Granero-Molto F, Weis JA, Miga MI, et al. Regenerative effects of transplanted mesenchymal stem cells in fracture healing. Stem Cells 2009;27:1887–1898.
13. Shapiro S, Borgens R, Pascuzzi R, et al. Oscillating field stimulation for complete spinal cord injury in humans: A phase 1 trial. J Neurosurg Spine 2005;2:3–10.
14. Pan L, Cirillo J, Borgens RB. Neuronal responses to an asymmetrical alternating current field can mimic those produced by an imposed direct current field in vitro. J Neurosci Res 2012;90:1522–1532.
15. Song B, Gu Y, Pu J, et al. Application of direct current electric fields to cells and tissues in vitro and modulation of wound electric field in vivo. Nat Protoc 2007;2:1479–1489.
16. Bardos DC, Thompson CJ, Yang YS, et al. Nonlinear cell response to strong electric fields. Phy Med Biol 2000;45:1965–1988.
17. Grant PF, Lowery MM. Electric field distribution in a finite-volume head model of deep brain stimulation. Med Eng Phy 2009;31:1095–1103.
18. Erickson CA, Nuccitelli R. Embryonic fibroblast motility and orientation can be influenced by physiological electric fields. J Cell Biol 1984;98:296–307.
19. Nuccitelli R, Erickson CA. Embryonic cell motility can be guided by physiological electric fields. Exp Cell Res 1983;147:195–201.
20. Graham DM, Huang L, Robinson KR, et al. Epidermal keratinocyte polarity and motility require Ca(2)(+) influx through TRPV1. J Cell Science 2013;126:4602–4613.
21. Carmeliet P, Dor Y, Herbert JM, et al. Role of HIF-1alpha in hypoxia-mediated apoptosis, cell proliferation and tumour angiogenesis. Nature 1998;394:485–490.
22. Kuhnert F, Mancuso MR, Shamloo A, et al. Essential regulation of CNS angiogenesis by the orphan G protein-coupled receptor GPR124. Science 2010;330:985–989.
23. Zhao Z, Walczysko P, Zhao M. Intracellular Ca2+ stores are essential for injury induced Ca2+ signaling and re-endothelialization. J Cell Physiol 2008;214:595–603.

24. Chang PC, Sulik GI, Soong HK, et al. Galvanotropic and galvanotaxic responses of corneal endothelial cells. J Formosan Med Assoc = Taiwan yi zhi 1996;95:623–627.
25. Li X, Kolega J. Effects of direct current electric fields on cell migration and actin filament distribution in bovine vascular endothelial cells. J Vasc Res 2002;39:391–404.
26. Zhao S, Zhu K, Zhang Y, et al. ElectroTaxis-on-a-Chip (ETC): An integrated quantitative high-throughput screening platform for electrical field-directed cell migration. Lab on a Chip 2014;14:4398–4405.
27. Zhao Z, Qin L, Reid B, et al. Directing migration of endothelial progenitor cells with applied DC electric fields. Stem Cell Res 2012;8:38–48.
28. Miyagi A, Chipot C, Rangl M, et al. High-speed atomic force microscopy shows that annexin V stabilizes membranes on the second timescale. Nat Nanotechnol 2016;11:783–790.
29. Zhao M, Bai H, Wang E, et al. Electrical stimulation directly induces pre-angiogenic responses in vascular endothelial cells by signaling through VEGF receptors. J Cell Sci 2004;117:397–405.
30. Zhang J, Calafiore M, Zeng Q, et al. Electrically guiding migration of human induced pluripotent stem cells. Stem Cell Rev Rep 2011;7:987–996.
31. Feng JF, Liu J, Zhang XZ, et al. Guided migration of neural stem cells derived from human embryonic stem cells by an electric field. Stem Cells 2012;30:349–355.
32. Lin F, Baldessari F, Gyenge CC, et al. Lymphocyte electrotaxis in vitro and in vivo. J Immunol 2008;181:2465–2471.
33. Wang E, Zhao M, Forrester JV, et al. Bi-directional migration of lens epithelial cells in a physiological electrical field. Exp Eye Res 2003;76:29–37.
34. Bai H, McCaig CD, Forrester JV, et al. DC electric fields induce distinct preangiogenic responses in microvascular and macrovascular cells. Arterioscler Thromb Vasc Biol 2004;24:1234–1239.
35. Sun Y, Do H, Gao J, et al. Keratocyte fragments and cells utilize competing pathways to move in opposite directions in an electric field. Curr Biol 2013;23:569–574.
36. Sato MJ, Kuwayama H, van Egmond WN, et al. Switching direction in electric-signal-induced cell migration by cyclic guanosine monophosphate and phosphatidylinositol signaling. Proc Natl Acad Sci U S A 2009;106:6667–6672.
37. Zhu K, Sun Y, Miu A, et al. cAMP and cGMP play an essential role in galvanotaxis of cell fragments. J Cell Physiol 2016;231:1291–1300.
38. Zhu K, Takada Y, Nakajima K, et al. Expression of integrins to control migration direction of electrotaxis. FASEB J 2019;33:9131–9141.
39. Sun Y, Reid B, Ferreira F, et al. Infection-generated electric field in gut epithelium drives bidirectional migration of macrophages. PLoS Biol 2019;17:e3000044.
40. Li Y, Gu Y, Wang H, et al. Electric pulses can influence galvanotaxis of dictyostelium discoideum. Biomed Res Int 2018;2018:2534625.
41. Ren X, Sun H, Liu J, et al. Keratinocyte electrotaxis induced by physiological pulsed direct current electric fields. Bioelectrochemistry 2019;127:113–124.
42. Tong J, Rezai P, Salam S, et al. Microfluidic-based electrotaxis for on-demand quantitative analysis of Caenorhabditis elegans' locomotion. J Vis Exp 2013:e50226.
43. Rezai P, Salam S, Selvaganapathy PR, et al. Effect of pulse direct current signals on electrotactic movement of nematodes Caenorhabditis elegans and Caenorhabditis briggsae. Biomicrofluidics 2011;5:44116–441169.
44. Kloth LC. Electrical Stimulation Technologies for Wound Healing. Adv Wound Care (New Rochelle) 2014;3:81–90.
45. Ennis WJ, Lee C, Gellada K, et al. Advanced technologies to improve wound healing: electrical stimulation, vibration therapy, and ultrasound-what is the evidence? Plast Reconstr Surg 2016;138:94S–104S.
46. Wolf-Goldberg T, Barbul A, Ben-Dov N, et al. Low electric fields induce ligand-independent activation of EGF receptor and ERK via electrochemical elevation of H(+) and ROS concentrations. Biochim Biophy Acta 2013;1833:1396–1408.
47. Swiontek T, Maiman D, Sances A, Jr., et al. Effect of electrical current on temperature and pH in cerebellum and spinal cord. Surg Neurol 1980;14:365–369.
48. Pakhomova ON, Khorokhorina VA, Bowman AM, et al. Oxidative effects of nanosecond pulsed electric field exposure in cells and cell-free media. Arch Biochem Biophy 2012;527:55–64.

Address correspondence to:
*Min Zhao, MD, PhD*
*Department of Ophthalmology & Vision Science,*
*Department of Dermatology*
*Institute for Regenerative Cures*
*University of California Davis*
*2921 Stockton Blvd.,*
*Sacramento, CA 9581*
*USA*

*Email:* minzhao@ucdavis.edu